PIEZO-AERO-ELASTICALLY COUPLED MODELING AND ANALYSIS OF ELECTRICAL POWER GENERATION AND SHUNT DAMPING FOR A CANTILEVERED PLATE

C. De Marqui, Jr[1]; A. Erturk[2]; D.J. Inman[3]
[1]Department of Aeronautical Eng., Engineering School of Sao Carlos, USP, SP, Brazil
demarqui@sc.usp.br
[2]Center for Intelligent Material Systems and Structures, Department of Eng. Science and Mechanics, Virginia Tech, VA, USA
erturk@vt.edu
[3]Center for Intelligent Material Systems and Structures, Department of Mechanical Eng., Virginia Tech, VA, USA
dinman@vt.edu

SUMMARY

The piezo-aero-elastic modeling of a cantilevered plate-like wing with embedded piezoceramics is presented for energy harvesting. The piezoelectrically coupled unsteady aeroelastic behavior of a composite cantilever is investigated. In addition to piezoelectric power generation, the effect of resistive shunt damping on the aeroelastic response of the generator wing is observed.

Keywords: Energy harvesting, piezo-aero-elasticity, piezoceramics

INTRODUCTION

Multifunctional structures are pointed out as a future breakthrough technology for Micro Air Vehicles (MAVs) and Unmanned Air Vehicles (UAVs) design. These structures perform additional tasks to its primary function [1]. Based on the concept of vibration-based energy harvesting the structure of an UAV or MAV can perform an additional task to its primary load carrying function: provide an additional source of electrical energy for these aircraft by converting vibrations available in their environment to electricity [2-6]. An additional electrical energy source can be useful to run small electronic components and ultimately to increase the flight time of the electrical power limited UAVs and MAVs. A possible source of energy for UAVs and MAVs is the mechanical vibration energy due to unsteady aerodynamic loads during the flight [7] and due to ground excitation in perching [8,9]. Piezoelectric transduction has received the most attention for vibration-based energy harvesting since four review articles have appeared in the last four years [2,4-6].

The literature of piezo-aero-elasticity includes the use of piezoelectric materials as sensors or actuators. Piezoceramic actuators and piezo-fiber-composite actuators are used to counteract aeroelastic effects in fixed-wing aircraft and helicopters [10-12]. Researchers have also used piezoelectric actuators for morphing aircraft [13]. Anton and

Inman [7] presented an experimental study on electrical power generation from the structural vibrations of a radio controlled glider in flight using piezoelectric patches at the roots of the wings and a piezoelectric cantilever inside the fuselage. Although aeroelastic vibrations constitute a useful additional energy source for UAVs and MAVs, a few papers have investigated the piezo-aero-elastic modeling of a generator wing at different airflow speeds.

In this work, piezo-aero-elastic modeling of a plate-like wing with embedded piezoceramics is presented. The coupled model is obtained from the combination an electromechanically coupled finite element (FE) model with an unsteady aerodynamic model. Classical plate theory is employed in the formulation of the FE model [14]. The unsteady aerodynamic model given here is based on a vortex lattice model [15]. In solving the piezo-aero-elastic equations of motion in time domain, the dependence between aerodynamic and electromechanical domains has to be addressed correctly. Therefore a predictor-corrector scheme [16] is used to solve the equations of motion. The main motivation is the investigation of the piezo-aero-elastic behavior of the generator wing. The piezoelectric shunt damping effect on the aeroelastic response of the generator wing due to electrical power generation is also investigated.

PIEZO-AERO-ELASTIC MODEL

The piezo-aero-elastic model is obtained from the combination an electromechanically coupled finite element (FE) model with an unsteady aerodynamic model.

Electromechanically Coupled Finite Element model

Using the linear-elastic constitutive relation for an isotropic substructure material and the linear electroelastic constitutive relation for a transversely isotropic piezoceramic material (used here in the plane-stress form [14].) the generalized Hamilton's principle for a piezoelectric energy harvester becomes,

$$\int_{t_1}^{t_2}\Bigg[\int_{V_s}\rho_s\delta\dot{\mathbf{u}}^t\dot{\mathbf{u}}dV_s+\int_{V_p}\rho_p\delta\dot{\mathbf{u}}^t\dot{\mathbf{u}}dV_p-\int_{V_s}\delta\mathbf{S}^t\mathbf{c}_s\mathbf{S}dV_s-\int_{V_p}\delta\mathbf{S}^t\mathbf{c}_p^E\mathbf{S}dV_p+\int_{V_p}\delta\mathbf{S}^t\mathbf{e}^t\mathbf{E}dV_p+\int_{V_p}\delta\mathbf{E}^t\mathbf{e}\mathbf{S}dV_p+$$
$$\int_{V_p}\delta\mathbf{E}^t\boldsymbol{\varepsilon}^S\mathbf{E}dV_p+\sum_{i=1}^{nf}\delta\mathbf{u}\left(x_i,y_i,t\right)\cdot\mathbf{f}\left(x_i,y_i,t\right)+\sum_{j=1}^{nq}\delta\varphi\left(x_j,y_j,t\right)q\left(x_j,y_j,t\right)\Bigg]dt=0 \tag{1}$$

where **u** is the vector of mechanical displacements, $\mathbf{c}_s$ is the 2-D elastic stiffness matrix obtained as function of the Poisson's ratio ν_s and the Young's modulus Y_s of the substructure material, **S** is the vector of mechanical strain components, **T** is the vector of mechanical stress components, **D** is the vector of electric displacement components, **E** is the vector of electric field components, **c** is the elastic stiffness matrix, **e** is the matrix of piezoelectric constants, $\boldsymbol{\varepsilon}$ is the matrix of permittivity components, superscript E and S denote that the parameters are measured at constant electric field and constant strain, respectively, ρ is the mass density, V is the volume, t denotes transpose when it is used as a superscript (otherwise it stands for the time) and an over-dot represents

differentiation with respect to time. Here and hereafter, subscripts s and p stand for the substructure and piezoceramic layers, respectively; $\mathbf{f}$ is the set of discrete mechanical forces applied at locations (x_i, y_i), q the set of discrete electric charge outputs extracted at locations (x_j, y_j), nf is the number of discrete mechanical forces, φ_j is the scalar electrical potential and nq is the number of discrete electrode pairs.

Typical piezoelectric energy harvesters, as depicted in figure 1, are designed to have cantilevered boundary conditions. The substructure and the piezoceramic layer of the unimorph piezoelectric energy harvester are assumed to be perfectly bonded to each other. The piezoceramic layer is bracketed by continuous and perfectly conductive electrodes with negligible thickness. A resistive load is considered in the electrical domain and the purpose is to estimate the power converted from the mechanical vibrations of the energy harvester plate. The electromechanically coupled FE model can be easily modified to represent a bimorph harvester as stated in the end of this section.

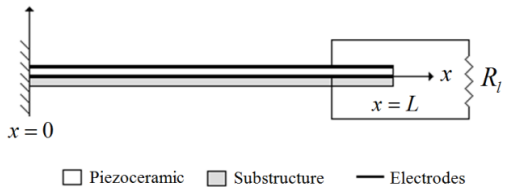

Figure 1. A unimorph piezoelectric harvester with clamped-free boundary conditions.

A rectangular finite element with four nodes and three mechanical degrees of freedom per node (namely the displacements u_x, u_y and u_z in x, y and z directions) is used to model the substructure and the piezoceramic layer. Based on the assumption that each finite element of the piezoceramic layer is completely covered with perfectly conductive electrodes, one electrical degree of freedom (voltage v_p across the electrodes) is added to the element for modeling the electrical domain of these elements.

Based on the Kirchhoff plate theory, shear deformations and rotary inertias of the finite elements are neglected and in-plane displacements (u_x and u_y) are assumed to be due to the bending (cross-section rotation) of the plate only. The displacement field is then

$$\mathbf{u} = \begin{Bmatrix} u_x \\ u_y \\ u_z \end{Bmatrix} = \begin{Bmatrix} -z\dfrac{\partial w}{\partial x} & -z\dfrac{\partial w}{\partial y} & w \end{Bmatrix}^t \tag{2}$$

where the displacement components u_x, u_y *and* u_z at a thickness level z from the reference (neutral) surface are given in terms of the transverse deflection (w) of the reference surface.

The mechanical strain components can be written as

$$\mathbf{S} = \begin{Bmatrix} S_x \\ S_y \\ 2S_{xy} \end{Bmatrix} = \begin{Bmatrix} \dfrac{\partial u}{\partial x} & \dfrac{\partial v}{\partial y} & \dfrac{\partial u}{\partial y} + \dfrac{\partial v}{\partial x} \end{Bmatrix}^t = -z \begin{Bmatrix} \dfrac{\partial^2 w}{\partial x^2} & \dfrac{\partial^2 w}{\partial y^2} & 2\dfrac{\partial^2 w}{\partial x \partial y} \end{Bmatrix}^t \tag{3}$$

The vector of nodal variables for the rectangular finite element can be defined as

$$\boldsymbol{\psi} = \left\{ w_1 \quad \theta_{x1} \quad \theta_{y1} \quad w_2 \quad \theta_{x2} \quad \theta_{y2} \quad w_3 \quad \theta_{x3} \quad \theta_{y3} \quad w_4 \quad \theta_{x4} \quad \theta_{y4} \right\}^t \tag{4}$$

where w_k is the transverse displacement for of node k, $\theta_{xk} = \partial w/\partial y\big|_{x_k, y_k}$ and $\theta_{yk} = -\partial w/\partial x\big|_{x_k, y_k}$ are the bending rotations. To derive the element matrices, the displacement field **u** described by Eq. (2) and consequently the strain components **S** described by Eq. (3) have to be expressed as functions of nodal variables. This is done expressing the transverse displacement (consequently the cross-section rotations) and the vector of curvatures in terms as,

$$\left\{ \frac{\partial w}{\partial x} \quad \frac{\partial w}{\partial y} \quad w \right\}^t = \mathbf{B}_{\boldsymbol{\eta}} \boldsymbol{\psi} \tag{5}$$

$$\left\{ \frac{\partial^2 w}{\partial x^2} \quad \frac{\partial^2 w}{\partial y^2} \quad 2\frac{\partial^2 w}{\partial x \partial y} \right\}^t = \mathbf{B}_{\boldsymbol{\kappa}} \boldsymbol{\psi} \tag{6}$$

where are $\mathbf{B}_{\boldsymbol{\eta}}$ and $\mathbf{B}_{\boldsymbol{\kappa}}$ are 3×12 matrices defined as interpolation functions.
The piezoceramics are assumed poled in the thickness direction (*z*-direction). Therefore the vector of electric field components can be expressed as,

$$\mathbf{E} = -\mathbf{B}_{\mathbf{E}} v_p \tag{7}$$

where $\mathbf{B}_{\mathbf{E}} = \left\{ 0 \quad 0 \quad \frac{1}{h_p} \right\}^t$.
The foregoing electrical relation and the previous mechanical equations (Eqs. 2 to 6) are used in the generalized Hamilton's principle given by Eq. (1) to give the element mass ($\mathbf{m}$) and stiffness ($\mathbf{k}$) 12 x 12 matrices, electromechanical coupling ($\boldsymbol{\theta}$) and external force ($\mathbf{f}$) 12 x 1 vectors and the scalar capacitance term (c_p). The global equations of motion are then obtained by assembling the element matrices resulting in the equations,

$$\mathbf{M}\ddot{\boldsymbol{\Psi}} + \mathbf{C}\dot{\boldsymbol{\Psi}} + \mathbf{K}\boldsymbol{\Psi} - \tilde{\boldsymbol{\Theta}} v_p = \mathbf{F} \tag{8a}$$

$$C_p \dot{v}_p + \frac{v_p}{R_l} + \tilde{\boldsymbol{\Theta}}^t \dot{\boldsymbol{\Psi}} = 0 \tag{8b}$$

where $\mathbf{M}$ is the global mass matrix ($n_m \times n_m$), $\mathbf{K}$ is the global stiffness matrix ($n_m \times n_m$) and $\tilde{\boldsymbol{\Theta}}$ is the global electromechanical coupling vector ($n_m \times 1$), C_p is the global capacitance term (scalar), $\mathbf{F}$ is the global vector of mechanical forces ($n_m \times 1$), $\boldsymbol{\Psi}$ is the global vector of mechanical coordinates ($n_m \times 1$), v_p the voltage output measure from the electrodes and R_l is the external resistive load. Equations (8a) and (8b) are modified

versions of the originally obtained equations. A transformation that accounts the presence of full electrodes bracketing the piezoceramics was used to modify the original equations [14]. Here, n_m and n_e, respectively, are the number of mechanical and electrical degrees of freedom of the harvester plate. In Eq. (8a), the global mechanical damping matrix ($n_m \times n_m$) is assumed to be proportional to the mass and stiffness matrices:

$$\mathbf{C} = \alpha\mathbf{M} + \beta\mathbf{K} \tag{9}$$

where α and β are the constant of proportionality.

This FE model is easily modified to represent a bimorph harvester (one substructure layer bracketed by two identical piezoceramic layers). The mass, stiffness and damping matrices have to consider the additional piezoceramic layer. For the bimorph in series connection case treated here the piezoceramic layers are assumed poled in the opposite direction, the effective electromechanical coupling vector is equal to that of one piezoceramic layer and the effective capacitance is one half of the capacitance of one piezoceramic layer [17].

Unsteady Aerodynamic Model

An unsteady vortex-lattice aerodynamic model (VLM) is used to obtain the loads over a cantilever plate-like wing [15]. A planar vortex ring is associated with each rectangular panel of the body itself and its wake. The aerodynamic loads on the wing are obtained by combining these singularities with the incompressible potential flow around the body. The leading segment of each planar vortex ring is placed at the quarter chord point of the panel. A control point is placed at the three-quarter chord of each panel for the verification of boundary condition that the normal component of the velocity of the fluid is zero across the solid boundaries of wing:

$$\left(\nabla\phi + \mathbf{v}_{motion} + \mathbf{v}_{wake}\right)\cdot\mathbf{n} = 0 \tag{10}$$

where $\Delta\phi$ is the gradient of the velocity potential corresponding to the perturbed velocity induced by the vortex singularities on the wing, $\mathbf{v}_{motion}$ is the velocity due to wing motion, $\mathbf{v}_{wake}$ is the velocity induced by the wake on the control points and $\mathbf{n}$ represents the normal direction to the surface of wing at the control points. The boundary condition has to be satisfied at each time step of this unsteady solution and this way the correct values for the circulation of vortex singularities are obtained.

The velocity induced at an arbitrary point by a straight segment of a vortex ring is given by the Biot-Savart law. This way the perturbed velocity induced by the vortex singularities on the wing depends on the geometrical characteristics of the aerodynamic grid (position of vortex ring corners and control points) and on the circulation values (the unknowns at each time step of the numerical solution scheme). If the surface of the plate-like wing has *m* panels ($m = R \times S$, where *R* and *S* are the number of panels along the chord and span, respectively) and consequently *m* vortex rings and control points, one can express the boundary condition in terms of the influence coefficients as,

$$\begin{bmatrix} a_{11} & a_{12} & \cdots & a_{1m} \\ a_{21} & a_{22} & \cdots & a_{2m} \\ \vdots & \vdots & \ddots & \vdots \\ a_{m1} & a_{m2} & \cdots & a_{mm} \end{bmatrix} \begin{Bmatrix} \Gamma_1 \\ \Gamma_2 \\ \vdots \\ \Gamma_m \end{Bmatrix} = -\begin{Bmatrix} \mathbf{v}_{motion_1} + \mathbf{v}_{wake_1} \\ \mathbf{v}_{motion_2} + \mathbf{v}_{wake_2} \\ \vdots \\ \mathbf{v}_{motion_m} + \mathbf{v}_{wake_m} \end{Bmatrix} \cdot \begin{Bmatrix} \mathbf{n}_1 \\ \mathbf{n}_2 \\ \vdots \\ \mathbf{n}_m \end{Bmatrix} \tag{11}$$

where a_{KL} is the influence coefficient that relates the circulation at the vortex ring *K* to the inner product of the perturbed velocity at point *L*. Both counters *K* and *L* can have values from 1 to $R \times S$. For example to scan all the vortex rings influencing the control point *K*, an inner scanning loop is need with the counter $L = 1 \rightarrow S \times R$. The unknowns in this linear set of equations are the circulations Γ_m of each vortex ring. The term $\mathbf{v}_{motion}$ is given by the free stream velocity plus velocities of the control points due to structural deformations of the wing. The free stream is always known; the velocities of the control points are determined by solving the electromechanically coupled FE model in time domain. The velocities induced by the wake $\mathbf{v}_{wake}$ are also obtained using Biot-Savart law. At each time step, new vortex rings are formed and shed from the trailing edge to the wake. The Kutta condition is satisfied imposing the circulation values of the most recently shed vortex rings at each time step as the same as those at the trailing edge (shedding vortices) in the previous time step. The circulation of the vortex rings on the wake remains unchanged and the wake carries no aerodynamic loads. The circulation values for the vortex rings placed on the wing are obtained from the solution of the linear system of equations given by Eq. (11). Therefore the aerodynamic load for each panel can be calculated from the unsteady Bernoulli equation.

Combination of the models and the numerical integration scheme

The equations of motion obtained from the FE formulation can be represented in modal domain as

$$\bar{\mathbf{M}}\ddot{\boldsymbol{\eta}} + \bar{\mathbf{C}}\dot{\boldsymbol{\eta}} + \bar{\mathbf{K}}\boldsymbol{\eta} - \boldsymbol{\Phi}^t\tilde{\boldsymbol{\Theta}}v_p = \boldsymbol{\Phi}_a^t\mathbf{F}_a \tag{12a}$$

$$C_p\dot{v}_p + \frac{v_p}{R_l} + \tilde{\boldsymbol{\Theta}}^t\boldsymbol{\Phi}^t\dot{\boldsymbol{\eta}} = 0 \tag{12b}$$

where $\boldsymbol{\eta}$ is the vector of modal coordinates, $\boldsymbol{\Phi}$ is the modal matrix (mass normalized so that the modal mass $\bar{\mathbf{M}}$ is the identity matrix), $\bar{\mathbf{C}}$ is the diagonal modal damping matrix, $\bar{\mathbf{K}}$ is the diagonal modal stiffness matrix, **F** is the vector of aerodynamic loads and $\boldsymbol{\Phi}_a$ is the modal matrix in aerodynamic coordinates. Note that in this equation $\boldsymbol{\Phi}_a$ accounts for the conversion of aerodynamic loads to the FE nodes.

In addition, structural displacements obtained at the nodes of FE mesh at each time step have to be obtained at the corners of vortex rings (aerodynamic mesh) for calculation of the aerodynamic loads. This way another transformation matrix is introduced to convert the modal coordinates to the corners of the vortex rings

$$\mathbf{x}_a = \boldsymbol{\Phi}_a^*\boldsymbol{\eta} \tag{13}$$

where $\mathbf{x}_a$ is the vector of aerodynamic coordinates and the matrices $\mathbf{\Phi}_a$ and $\mathbf{\Phi}_a^*$ are interpolated in this work using surface splines.
The equations of motion can be written as a system of $2n$ + 1 first order ordinary-differential equations, where n is the number of modes taken into account in the solution. The $2n+1$ ordinary-differential equations are then solved using the Adams-Bashforth-Moulton predictor-corrector scheme that accounts for the interaction between aerodynamic and electromechanical domains [16].

RESULTS

This section presents the piezo-aero-elastic behavior of a cantilevered plate-like wing with embedded piezoceramics. Two identical layers of (PZT-5A) are embedded into the top and on the bottom of the plate. Conductive electrodes bracketing the piezoceramic layers are connected in series to a resistive electrical load as depicted in figure 2. It is important to mention that the electromechanical coupled FE model has been successfully verified [14] against the analytical results obtained from the closed-form solution given by Erturk and Inman [17] for a unimorph harvester under base excitation and also against the analytical and experimental results for a bimorph harvester with a tip mass under base excitation presented by Erturk and Inman [18]. The aeroelastic model (with no piezoceramic added) has been verified against the numerical results presented by Tang et al [19].

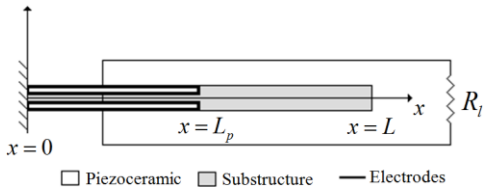

Figure 2. Generator wing with embedded piezoceramics (series connection).

The dimensions of the plate-like wing used in this work are 1200 × 240 × 3 mm^3. The identical embedded piezoceramic layers have the same width as the wing chord. The embedded piezoceramics layers cover 30% of the wing span (from the root to the tip) and each one has a thickness of 0.5 mm. The geometric and material properties of the wing (aircraft aluminum alloy Al 2024-T3) are presented in Table 1.

Table 1. Geometric and material properties of the aluminum wing

Length of the wing (mm)	1200	Mass density (kg/m^3)	2750
Width of the wing (mm)	240	Proportional constant – α (rad/s)	0.1635
Thickness of the wing (mm)	3	Proportional constant – β (s/rad)	4.1711 x 10^{-4}
Young's modulus (GPa)	70.0		

The material and electromechanical properties for PZT-5A are given in Table 2. The plate-type formulation given here requires more than what is provided in the manufacturer's data sheet (see, for instance, the properties required for the calculation of the plane-stress elastic, piezoelectric and dielectric components in [14]). Therefore, the 3-D properties of PZT-5A displayed in Table 2 are used here.

Table 2. Material and electromechanical properties of PZT-5A

Mass density (kg/m^3)	7800	c_{33}^E (GPa)	110.9
Permittivity (nF/m)	$1800\times\varepsilon_0$	c_{66}^E (GPa)	22.7
c_{11}^E, c_{22}^E (GPa)	120.3	e_{31}, e_{32} (C/m^2)	-5.2
c_{12}^E (GPa)	75.2	e_{33} (C/m^2)	15.9
c_{13}^E, c_{23}^E (GPa)	75.1		

The mode sequence and the undamped natural frequencies for the plate-like wing obtained from the FE model for short-circuit conditions (very low load resistance) is 1st B (1.68 Hz), 2nd B (10.46 Hz), 1st T (16.66 Hz), 3rd B (27.74 Hz) and 2nd T (48.65 Hz). Here B and T stand for the bending modes and torsion modes, respectively. The span-wise elastic axis and the center of gravity are coincident at 50% of chord.

One can observe in figures 3a and 3b the piezo-aero-elastic behavior of the generator wing for the short-circuit conditions. Figure 3a shows the frequency content of the five modes considered during the simulation. For the airflow speeds smaller than 20 m/s the frequencies are still similar to the undamped natural frequencies (which is given for the case without airflow). Increasing airflow speed results in coupling among the modes. For the airflow speed of 40 m/s the modes are coupled at the flutter frequency (12.2 Hz). The motion of the plate-like generator wing at the flutter speed is quite dominated by a second bending mode with some torsion coupling.

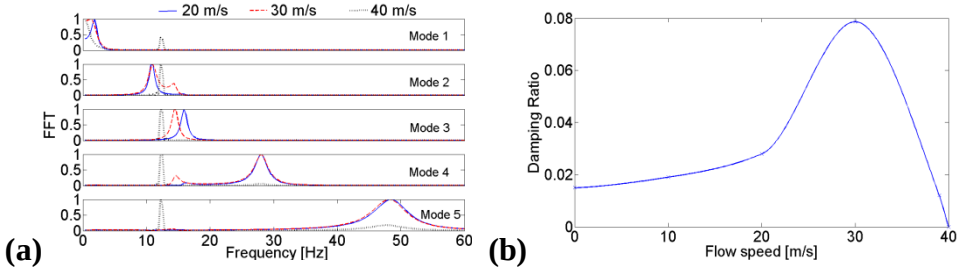

Figure 3. (a) Frequency content for three different flow speeds; (b) variation of total (structural and aerodynamic) damping ratio with increasing flow speed.

The variation of total damping ratio (summation of structural damping and aerodynamic damping) for the second vibration mode with increasing airflow speed is presented in figure 3b. Damping has a major effect in vibration-based power harvesting. Therefore larger mechanical amplitudes and consequently larger power outputs are expected for large aerodynamic loads and low damping which is the case for airflow speeds around the flutter condition.

The time history of power output for the flutter speed is shown in figure 4a. The power output increases as the value of load resistance is increased from $R_l = 10^2\ \Omega$ to $R_l = 10^4\ \Omega$ as can be observed in the enlarged view of figure 4a. Power output is continuously extracted over the time in this underdamped case. Clearly the value of load resistance $R_l = 10^4\ \Omega$ provides the maximum power output among the set of load resistances considered here. Note that the time history with the largest power for this load resistance shows a decaying behavior which is due to the strong shunt damping

effect of power generation for $R_l = 10^4\ \Omega$, what can also be verified in figure 4b. If R_l is increased to $10^5\ \Omega$, the amplitude of power output decreases. When the load resistance is further increased to $R_l = 10^6\ \Omega$ the power output is considerably reduced to values similar to the values obtained for $R_l = 10^2\ \Omega$ (enlarged view in figure 4a).

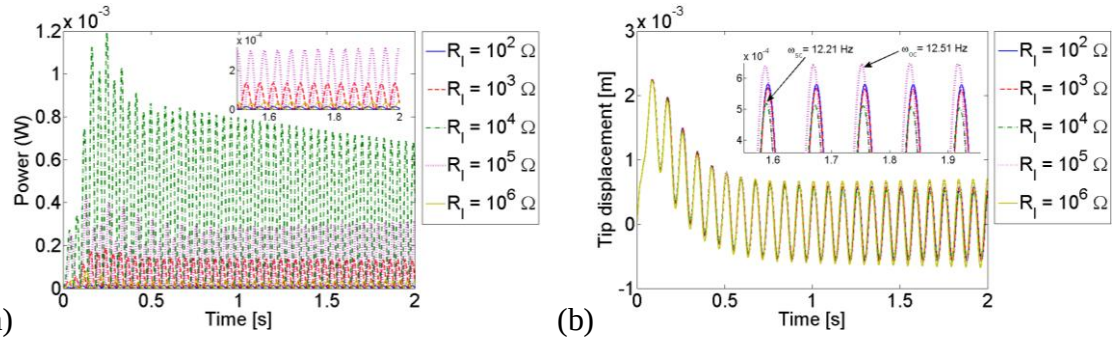

(a) (b)

Figure 4. (a) Power output for five different values of load resistance at the flutter speed; (b) tip displacement for five different values of load resistance at the flutter speed.

CONCLUSIONS

It is observed that the aeroelastic behavior as well as vibration-based energy harvesting are strongly modified by the variation of aerodynamic damping. Clearly the most favorable conditions for power harvesting using the plate-like generator wing occur for airflow speeds higher than 30 m/s and especially for very low values of aerodynamic damping. At the flutter speed, the aerodynamic damping vanishes and the oscillations are persistent. Although this condition is avoided in a real aircraft, this is the best condition as a concept demonstration for the generator wing investigated here.

In addition to the benefit of electrical power generation from aeroelastic vibrations, the resistive shunt damping effect is observed. An optimum value of load resistance (among the values considered in this work) is obtained and the amplitude of motion is reduced especially for the loads yielding larger power output. Therefore, it is possible to define a short-circuit flutter speed and a slightly larger open-circuit flutter speed.

ACKNOWLEDGEMENTS

The authors gratefully acknowledge the support of the Air Force Office of Scientific Research MURI under grant number F 9550-06-1-0326 “Energy Harvesting and Storage Systems for Future Air Force Vehicles” monitored by Dr. B. L. Lee. The authors also gratefully acknowledge the support of CAPES (Brazil).

References

1. Dodemant L R 2007 *Multifunctional structures for spacecraft:Embedded lithium-ion batteries* MSc Thesis Cranfield University
2. Sodano H A, Inman D J and Park G 2004 A review of power harvesting from vibration using piezoelectric materials *The Shock and Vibration Digest* 36 197-205
3. Beeby S P, Tudor M J and White N M 2006 Energy harvesting vibration sources for microsystems applications *Measurement Science and Technology* 13 R175-R195

4. Priya S 2007 Advances in energy harvesting using low profile piezoelectric transducers *Journal of Electroceramics* 19 167–184
5. Anton S R and Sodano H A 2007 A review of power harvesting using piezoelectric materials 2003-2006 *Smart Materials and Structures* 16 R1-R21
6. Cook-Chennault K A, Thambi N and Sastry A M 2008 Powering MEMS portable devices – a review of non-regenerative and regenerative power supply systems with emphasis on piezoelectric energy harvesting systems *Smart Materials and Structures* 17 043001
7. Anton S R and Inman D J 2008 Vibration energy harvesting for unmanned air vehicles *Smart Structures and Materials 2008: Active and Passive Smart Structures and Integrated Systems II*; Proc. SPIE 6928
8. Magoteaux K C, Sanders B and Sodano H A 2008 Investigation of energy harvesting small unmanned air vehicle Smart Structures and Materials 2008: Active and Passive Smart Structures and Integrated Systems II Proc. SPIE 6928
9. Erturk A, Renno J M and Inman D J 2008 Modeling of piezoelectric energy harvesting from an L-shaped beam-mass structure with an application to UAVs *Journal of Intelligent Material Systems and Structures* 20 529-544
10. Friedmann P P 1998 Rotary-wing aeroelastic scaling and its application to adaptive materials based actuation *39th AIAA/ASME/ASCE/AHS/ASC Structures, Structural Dynamics, and Materials Conference and Exhibit, and AIAA/ASME/AHS Adaptive Structures Forum*
11. Librescu L. and Na S 2000 Vibration and dynamic response control of elastically tailored nonuniform adaptive aircraft wings *41st AIAA/ASME/ASCE/ AHS/ASC Structures, Structural Dynamics, and Material Conference and Exhibit*
12. Giurgiutiu V 2000 Review of Smart-Materials Actuation Solutions for Aeroelastic and Vibration Control *Journal of Intelligent Material Systems and Structures* 11
13. Bilgen O, Kochersberger K, Diggs E, Kurdila A and Inman D J 2007 Morphing wing micro-air-vehicles via macro-fiber-composite actuators *48th AIAA/ASME/ASCE/AHS/ASC Structures, Structural Dynamics, and Materials Conference*
14. De Marqui Jr C, Erturk A and Inman D J 2009 An Electromechanical Finite Element Model for Piezoelectric Energy Harvesters *Journal of Sound and Vibration* (in press)
15. Benini G R, Belo E M and Marques F D 2004 Numerical Model for the Simulation of Fixed Wings Aeroelastic Response *Journal of the Brazilian Society of Mechanical Sciences & Engineering* 26 129-136
16. Lambert J D 1991 *Numerical Methods for Ordinary Differential Systems: The Initial Value Problem* (Chichester: Wiley)
17. Erturk A and Inman D J 2008 A distributed parameter electromechanical model for cantilevered piezoelectric energy harvesters *ASME Journal of Vibration and Acoustics* 130 041002
18. Erturk A and Inman D J 2009 An experimentally validated bimorph cantilever model for piezoelectric energy harvesting from base excitations *Smart Materials and Structures* 18 025009
19. Tang D, Dowell E H and Hall K C 1999 Limit cycle oscillations of a cantilevered wing in low subsonic flow AIAA Journal 37 364-371